Articles in PresS. Am J Physiol Regul Integr Comp Physiol (February 13, 2008). doi:10.1152/ajpregu.00829.2007

CIRCADIAN RHYTHM DISORGANIZATION PRODUCES PROFOUND CARDIOVASCULAR AND RENAL DISEASE IN HAMSTERS

Tami A. Martino[1,2,3], Gavin Y. Oudit[1,2], Andrew M. Herzenberg[1], Nazneen Tata[1], Margaret M. Koletar[3,4], Golam M. Kabir[2], Denise D. Belsham[1,3], Peter H. Backx[2,3], Martin R. Ralph[3,4*] & Michael J. Sole[1,2,3*]

1. University Health Network, Toronto, Ontario
2. Heart and Stroke/Richard Lewar Centre for Cardiovascular Excellence, University of Toronto, Ontario, Canada
3. Departments of Physiology, Medicine, Psychology, University of Toronto, Canada
4. Centre for Biological Timing and Cognition, University of Toronto, Ontario, Canada

*Correspondence to:
Michael J. Sole, 4N-488 Toronto General Hospital, 585 University Avenue, Toronto, Ont., Canada, M5G 2N2; E-mail: michael.sole@uhn.on.ca. Or,

Martin R. Ralph, Centre for Biologic Timing and Cognition, Department of Psychology, SSH 4017, University of Toronto, Ontario, Canada; E-mail: ralph.mr@gmail.com

Short Title: Circadian Disorganization Causes Heart Disease

Acknowledgements. We thank Dr. Z. Jia, J. Chalmers, O. Rawashdeh, and K. Varano for technical assistance. We are grateful for the support of the A. Ephriam and Shirley Diamond Cardiomyopathy Research Fund, a grant from the Heart and Stroke Foundation of Ontario (T4479) to M.J.S, and a grant from the Natural Sciences and Engineering Research Council of Canada to M.R.R. T.A.M. acknowledges the Heart and Stroke Foundation of Ontario, and the Heart and Stroke Richard Lewar Centre for Cardiovascular Excellence.

Abstract

Sleep deprivation, shift work, and jet lag all disrupt normal biological rhythms and have major impacts on health; however, circadian disorganization has never been shown as a causal risk factor in organ disease. We now demonstrate devastating effects of rhythm disorganization on cardiovascular and renal integrity, and that interventions based on circadian principles prevent disease pathology caused by a short period mutation (*tau*) of the circadian system in hamsters. The point mutation in the circadian regulatory gene, casein kinase-1-ε (*ck1ε*^{tau}) produces early-onset circadian entrainment with fragmented patterns of behavior in +/*tau*–heterozygotes. Animals die at a younger age with cardiomyopathy, extensive fibrosis, and severely impaired contractility; they also have severe renal disease with proteinuria, tubular dilation, and cellular apoptosis. On light cycles appropriate for their genotype (22 hr), cyclic behavioral patterns are normalized, cardiorenal phenotype is reversed, and hearts and kidneys show normal structure and function. Moreover, hypertrophy does not develop in animals whose SCN was ablated as young adults. Circadian organization therefore is critical for normal health and longevity whereas chronic global asynchrony is implicated in the etiology of cardiac and renal disease.

Keywords : Circadian, Diurnal, Tau Hamsters, Heart Disease, Renal Disease, SCN

Introduction

It has been recognized for decades that circadian rhythms play a dramatic role in the regulation of cardiovascular physiology (7, 16). Moreover, adverse cardiac events (e.g. heart attacks, stroke) show significant day/night (diurnal) variations in both incidence and severity(16), and rhythm disruption is found commonly in patients with sleep apnea, in shift workers, and in transmeridian flight crews, all of whom show higher than average prevalence of cardiovascular disease(2, 6). In animal models, disruption of diurnal rhythms increases mortality in cardiomyopathic hamsters(19) and exacerbates pressure overload myocardial hypertrophy in aortic banded mice(15).

Circadian rhythm disruption also has been linked with reduced longevity in golden hamsters carrying the circadian period mutation, *tau(11)*. The mutant allele reduces circadian period from about 24h in the wild type to about 22h in *tau/+* heterozygotes (20). Importantly, it is the heterozygotes whose longevity is compromised. When these animals are entrained by 24h LD cycles they exhibit phase advanced onsets of nocturnal behavior with significant fragmentation of diurnal activity(18). Conversely, longevity is increased in aged animals whose disturbed rhythms are reconsolidated by successful grafting of hypothalamic tissue containing the suprachiasmatic nucleus (SCN)(11). Nonetheless, other than the changes in rhythm integrity, the mechanisms underlying the effects on life expectancy have not been explored. Therefore, despite the acknowledged importance of rhythms in health and disease, there are virtually no experimental data prospectively demonstrating a causal link between circadian dysregulation and organ pathology. In this study we hypothesize that altered circadian organization plays a role in genesis of severe cardiac and renal disease, leading to early death in +/tau mutant hamsters.

Materials and Methods

Animal housing and locomotor behavior recording. All animals are housed at the University of Toronto zoology animal facility. This investigation conforms to the *Guide for Care and Use of Laboratory Animals* published by the US National Institutes of Health (NIH Publication No. 85-23, revised 1996), and the guidelines of the Canadian Council on Animal Care. The hamsters (*Mesocritetus auratus; tau*) have been maintained in the breeding colony in a LD 14:10 cycle since 1991, and the colony is outbred every second generation with wildtype obtained from Charles River Laboratories, Quebec. Activity is recorded from individual cages equipped with running wheels as required using Dataquest II data acquisition system coupled with ActiView Biological Rhythm Analysis Version 1.2 (Minimitter Co., Inc., Bend, Oregon). Genotype is confirmed by PCR analysis of the *casein kinase 1 epsilon* gene.

SCN ablation. Electrolytic lesions of the SCN are produced using electrodes aimed at the SCN place stereotaxically on midline under deep pentobarbital anesthesia. Coordinates are: AP +0.6 mm from bregma and -0.8 mm from dura. Lesions are small, and nearby structures (medial preoptic N.; subparaventricular zone, optic chiasm) are spared. Placement is verified by the lack of 24h rhythmicity in subsequent behavioral records and by histologic examination.

Echocardiography. Echocardiography is performed in a blinded manner on all hamsters at 4 and at 17 months of age. All animals are housed on a 24h LD cycle (14:10) throughout, or for those on alternative cycles they are returned to LD 14:10 3 weeks prior to final cardiovascular assessments. Animals are anesthetized with 2% isoflurane gas delivered through a nose cone, and are maintained at a body temperature of 37^0C using a heating pad. Transthoracic echocardiography is performed with Sequoia (Acuson, Mountain View, California) using a 13 MHz linear array probe. 2D M-mode images are acquired while the animal is in a semi-conscious state (0.75% Isoflurane) using High Resolution Zoom with a sweep speed of 200 mm/s, from the short axis view at the papillary muscle level. Measurements include LV end-diastolic (LVEDD) and end-systolic (LVESD) diameter, LV

diastolic anterior and posterior wall thickness (AWT and PWT), % fractional shortening (%FS), and heart rate.

Hemodynamic studies. *In vivo* hemodynamic measurements are performed in a blinded manner on animals anesthetized with 1.5% isoflurane gas. Body temperature and heart rate are continuously monitored and maintained. The right common carotid artery is exposed, and cannulated using a 1.4 French microtip catheter (Millar Inc., Houston), which is then fed to the proximal aorta and left ventricle for respective measurements. Data is acquired using the MP100 hardware imaging system, and analyzed using Acqknowledge version 3.7.3 (BIOPAC Systems, Inc.). Data is analyzed for aortic systolic and diastolic blood pressure (SBP, DBP), and mean arterial blood pressure (MABP), and LV pressure measurements (LVESP, LVEDP), and the maximum and minimum first derivatives of LV pressure (LVdP/dT max, min).

Histology and pathological assessment of hamsters. Animals are anesthetized, euthanized, and tissues collected. For histological assessment, tissues are fixed in 10% formalin and paraffin-embedded. Heart sections taken at the level of the papillary muscle are stained with hematoxylin and eosin (H&E, Sigma), Massons Trichrome, or Picrosirius Red (PSR, Fluka). Kidney sections are stained with H&E, PSR, or Period Acid Schiff. We determined in a blinded manner the general tissue morphology, myocyte cross sectional area (MCSA), and extent of interstitial fibrosis. Sections are digitally imaged using the Nikon microphot-FXA microscope, along with the Nikon ACT-1 version 2.62, or ImageJ 1.33u (National Institute of Health, USA) software.

Electron Microscopy glomerular analyses. Glomerulosclerosis, tubular hyperplasia, and renal fibrosis are assessed using pathologic cross-sections. For electron microscopy of renal glomeruli, kidneys are fixed in buffered 1% glutaraldehyde-4% formaldehyde, postfixed in 1% osmium tetroxide, and embedded in Epon-araldite. Ultrathin sections stained with uranyl acetate and lead citrate are examined using a transmission electron microscope (1200EX-II; Jeol Peabody, MA).

In Situ End Labeling Assay (TUNEL). DNA damaged cells are detected by terminal uridine deoxynucleotidyl transferase dUTP nick end labeling (TUNEL) assay, adapted to an automated in-situ hybridization instrument (Discovery™ Ventana Medical Systems, Inc. Tuscon, AZ. USA). We use 5μm thick deparaffinized tissue sections, digestion with Protease I (Ventana Medical), recombinant terminal deoxynucleotidyl transferase (Tdt) (GIBCO BRL), and Biotin 16-dUTP (Roche Diagnostics), in accordance with well-established protocols. Colormetric visualization uses avidin-HRP and 3,3'-diaminobenzidine (DAB), with hematoxylin counterstain.

Immunohistochemistry. Immunohistochemistry for CD3 (Dako, Carpinteria, Ca, USA.) is performed on the NEXES™ auto-immuno stainer (Ventana Medical Systems, Tuscon, Arizona, USA) at a dilution of 1:200, in accordance with the manufacturers specifications. Immunodetection is carried out using a 1:100 dilution of biotinylated anti rabbit IgG (Vector Laboratories, Burlingame, CA, USA) and the Ventana DAB (3-3'- Diaminobenzidine) Detection System. Tissue sections are heated prior to immunostaining, and endogenous biotin blocked (Ventana Avidin/Biotin Block), and finally counterstained with haematoxylin.

Proteomics and Mass Spectrometry; Protein Analyses, SDS-PAGE, trypsin digestion, MS/MS by LC-ESI-ION TRAP. Protein content of each sample is determined using the Bradford Assay method (Bio-Rad Laboratories). Urinary protein content is analyzed on 10-20% tricine gels (Invitrogen) stained with Coomassie dye for 20 min. Selected bands are prepared for MS/MS by excision from the gel, and digested overnight in 50ul buffer containing 50mM HN4HCO3, 10% acetonitrile, and 10ng/ul sequencing grade trypsin (Roche). The MS/MS analysis of tryptic peptides is performed using a LCQ DECA XP ion trap (Thermo Finnigan, CA, USA). Buffer A for liquid chromatography contains 0.1% formic acid, and buffer B contains 99.9% acetonitrile and 0.1% acetic acid. Samples are injected at a rate of 10ul/min onto a Vydac reverse phase column (0.2x150mM, Grace Vydac, Hesperia, CA, USA) over 5 min in 5% buffer B, using an Agilent 1100 Series CAP-LC (PaloAlto, CA, USA). Peptides are eluted over a 10-65% buffer B gradient for 40 min at a rate of 2ul/min for detection by LCQ DECA XP mass spectrometry. Data analysis is performed by Sequest software (Lisle, IL, USA) with raw files searched against hamster,

murine, and human databases on NCBI (www.ncbi.nlm.nih.gov/). Positive identifications are made when 2 or more peptides with Xcorr >2.5 (+2ions) or >3.7 (+3 ions) match to the same protein. Protein identification is validated as required, using Western blot analysis on nitrocellulose membrane and chemiluminescent detection (Amersham Biosciences).

Plasma Biochemistry and Kidney Function Analysis. Blood samples are collected from anesthetized hamsters at ZT12-16 and 200 µl of plasma is used for measurement of plasma Na^+, K^+, Cl^-, ionized Ca (Ca^{2+}), lactate, glucose, urea and creatinine using a Stat Profile M7 Analyzer (Nova Biomedical Corp., Waltham, Massachusetts, USA).

Statistical Analyses. Data are expressed as mean +/- SEM. Statistical comparisons are made either by use of the independent Student's T-test for comparing individual groups or by one-way ANOVA followed by Tukey's multiple test for comparisons of more than 2 groups. Analysis is performed using SPSS statistical software (v.12.0.0). Results of $p<0.05$ are considered statistically significant.

Results

We postulated that chronic circadian disorganization like that seen in *tau*/+ animals on 24h LD cycles results in pervasive physiological impairments leading to early demise. To test this we focus specifically on the cardiovascular system where robust diurnal or circadian cycling of gene expression already has been shown(14, 21, 23, 24), and wherein a pathological effect of rhythm disturbance has been implicated in human beings(7, 16). All animals are genotyped using an ear tip for DNA analyses (Fig. 1A, genotyping) and phenotyped using conventional behavioral analyses (Fig. 1B *tau*/+, left; wildtypes, right).

We first perform autopsy examination of animals at 17 months of age, close to the limit of the shortened lifespan of the *tau*/+ hamsters(11). This reveals a marked cardiomyopathy consistent with our hypothesis. Histopathology reveals extensive interstitial fibrosis (Fig. 1Ci) and widespread collagen deposition in the extracellular matrix (Fig. 1Di) in the myocardium of *tau*/+ animals as compared to the wildtypes. The adverse remodeling is digitally quantified and is significantly increased in *tau*/+ hearts compared to wild type (Fig.

1E and Table 1). We recognize that an ideal method for quantification of myocardial fibrosis is performed by measuring the volume fraction of myocardium occupied by collagen tissue; the pixels approach only estimates the extent of fibrosis that occurs. However, volume fractionation was not feasible in the current setting, and moreover, since the interstitial fibrosis is so pervasive in the *tau*/+ hearts and virtually nonexistent in all the other groups the rough measure should suffice to show relative intensity and scale. We also note widespread myocyte hypertrophy in *tau*/+ hearts, as evidenced by pathologic staining (Fig. 1Ci, 1Di), and by quantification (Fig. 1F and Table 1). In addition, the heart weight (Fig. 1G) and heart weight:body weight ratios (Fig. 1H) are significantly increased in *tau*/+ hearts (also see Table 1). Thus collectively, these findings show the development of obvious hypertrophy and extensive pathologic remodeling in the *tau*/+ heart.

To evaluate cardiac function we perform *in vivo* catheterization and hemodynamics, and document significant deterioration in *tau*/+ heart versus wildtype (Table 1). This includes: (1) markedly decreased systolic, diastolic, and mean arterial blood pressure ($P<0.01$) indicative of hypotension in the *tau*/+ animals; (2) significantly increased left ventricular end diastolic pressure (LVEDP) consistent with diastolic dysfunction in the heart ($P<0.01$); and (3) reduced (40%) dP/dtmax and -dP/dtmax values showing significantly impaired myocardial contractility ($P<0.01$). Impaired cardiac function is confirmed using transthoracic echocardiography (Table 1). Left ventricular end diastolic (LVEDD) and systolic (LVESD) dimensions are significantly increased, and ventricular fractional shortening (FS), a mathematical measure of systolic function, is greatly reduced from 46.3% (wt) to 29.7% (*tau*/+) ($P<0.01$). Flow parameters measured as velocity of circumferential shortening (VCFc) and peak aortic velocities (PAV) are also significantly reduced, consistent with the hypotension ($P<0.01$). Thus these data show that in addition to profound pathologic findings in the hearts of *tau*/+ animals, the physiology reflects severe myocardial hypertrophy and dysfunction leading to cardiomyopathy and heart failure.

We then exclude the possibility that the cardiac phenotype in the *tau*/+ animals is due to a pleiotropic gene effect. Consistent with this notion, cardiopathology was restricted to the heterozygotes. The homozygous *tau/tau* hamsters (period = 20 hr) retain consolidated patterns of behavior and are unable to synchronize with 24 hr days (and thus do not show the same circadian dysregulation as the *tau*/+ hamsters do), and importantly, do not develop

pathology nor declining cardiac function like heterozygotes. Furthermore, young *tau*/+ hamsters (4 months of age and easily assessed by actigraphy) appear healthy, with all cardiovascular parameters including cardiac pathology, hemodynamics, and echocardiography similar to the wild types (Table 2, also see Figure 4 below). Although this does not definitively disclude congenital conditions, they are certainly not obvious. Moreover, it suggests the cardiomyopathy that develops in *tau*/+ animals does so only over an extended period of circadian dysregulation. In the aggregate then, abnormal circadian entrainment appears to act as a procardiomyopathic stimulus and the heart decompensates over time.

We also measure plasma biochemistry and detecte elevated K+ and creatinine levels specifically in the 17 month old *tau*/+ mutants (Table 3) but no changes in other plasma values including normal glucose levels. These findings suggest that the *tau*/+ animals with severe heart disease may also have underlying kidney disease. Indeed, we observe severe renal pathology in the *tau*/+ mutants including proximal tubular dilatation with degenerative and regenerative changes; the glomeruli show ischemic change (Fig. 2A), and active fibrosis or collagen deposition throughout the renal cortex (Fig. 2B). However, the basement membrane thickness appears normal and there are no immune-type electron dense deposits thus indicating that the renal disease is primary in origin and not likely due to infectious nor autoimmune processes (Fig. 2C).

The aging *tau*/+ also exhibit proteinuria as compared to all other groups. This is analyzed by determining protein concentration in the urine of all the tau hamster phenotypes, and at both early (4 month) and late (17 month) ages (Fig. 3A). Next, we ran SDS-PAGE electrophoresis, revealing the presence of both high and low molecular weight proteins in urine of the aging (17 month) *tau*/+ animals (Fig. 3B). These findings are consistent with the high protein concentrations in the urine, and with the severe renal phenotype. We noted one gel band on SDS-PAGE that consistently appeared in the urine samples analyzed from 17 month tau/+ animals. This band appeared at MW ~15kDa (see lower arrow on right side of gels, Fig. 3B). To identify the protein in this band, we use mass spectrometry proteomics. The gel band is excised, and trypsin digested, and injected by electron spray ionization (ESI) into an LCQ DECA XP ion trap mass spectrometer (MS)/MS. The identity is confirmed by database searching against hamster, murine, and human databases, and by molecular mass

comparisons, and detection from multiple samples. The ~15kDa band was identified by MS/MS as cytochrome c, which is normally located in the mitochondria of cells. However, release of cytochrome c from the inner mitochondrial membrane results in nuclear apoptosis. A representative MS/MS spectrum for cytochrome c is shown (Fig. 3C).

As cytochrome c release from mitochondria is indicative of cellular apoptosis, this provides a possible mechanism for renal tissue damage in the *tau*/+. Thus we further investigate by assaying the renal tissue for apoptosis, using the TUNEL assay, a common method for detecting DNA fragments resulting from apoptotic signaling cascades. We observe positive staining in *tau*/+ mutant kidney (Fig. 3D), indicative of apoptosis, and consistent with our findings of urinary cytochrome c, and with the severe renal phenotype. Clinically, these findings are interesting because cardiovascular disease and kidney disease very often are associated in humans.

We then test the notion that circadian rhythm disruption alone can be responsible for the abnormal cardiorenal phenotype, by maintaining *tau*/+ hamsters from 4 months of age (a time at which heart disease is not yet evident). In one experiment we raise animals in a phenotype-appropriate 22h light:dark cycle (LD 12:10). We retained 10 hr of dark to ensure that a consolidation of nocturnal type behavior is not an artifact of exposure to very short nights. Behavioral analysis demonstrates that temporal profiles in *tau*/+ are similar in LD12:10 as in DD where the endogenous period of ca. 22h is expressed (Fig. 4A). At 17 months of age, animals are reexamined and remarkably the abnormal cardiac and renal phenotypes are both completely absent. This is confirmed by gross morphology, histopathology, plasma biochemistry, urinalysis, and cardiac function using echocardiography and *in-vivo* hemodynamics. Thus, all measurements taken from the *tau*/+ group on 22h days are similar to the wild type and are statistically and "clinically" different from *tau*/+ group raised on 24h days (for pathology see Figs. 4B-D; for pathophysiology see Figs. 4E-H); data for 22h *tau*/+ are listed in Table 1).

In a second experiment, we ablate the SCN thereby removing the influence of the master circadian oscillator over the peripheral oscillators in heart and kidney. Physiological parameters are not measures in these animals as the circadian phase of cardiovascular rhythm can not be determined. However, heart weight to body weight ratios are significantly higher in *tau*/+ than wild type animals held in the LD14:10 condition, as expected. However,

arrhythmic, SCN lesioned *tau*/+ animals have significantly lower ratios than the intact *tau*/+ animals, and are not different from wildtype (Fig. 5).

Discussion

The data presented here are consistent with the general hypothesis that diurnal cycling plays a key role in organ growth and renewal and that disruption is a key contributor to disease. Demonstration of abnormal entrainment in *tau*/+ hamsters leading to cardiomyopathy is novel. We postulate that prolonged external endocrine and/or neural cues, through the daily resetting of the clock, play a critical role in triggering the procardiomyopathic response. The discovery of a concomitant renal pathology suggests that circadian disorganization has pervasive effects on organ health. Certainly the presence of molecular circadian clocks has been demonstrated in several peripheral tissues(5). A recent report that circadian clocks provide temporal organization for the proliferation of renal tubular epithelial cells(12), may give us perhaps some insight into the origins of the urinary cytochrome c marker, cortical cell apoptosis, and renal pathology.

It is important to recognize that the key factor in producing cardiovascular disease may not be disruption of the tissue molecular clock *per se* but the global disturbance or desynchrony that results from the presence of oscillators that are attempting to operate at two distinct periods. That is, in the *tau*/+ heterozygotes, rhythms in peripheral tissues are being produced not only by the intrinsic 22 hour molecular oscillator but also by 24 hour signals from the SCN, which is being driven by the LD cycle. When the SCN is influenced by a 22 hour LD cycle, cardiovascular disease does not develop, as our data show.

The alternative, that the mutated casein kinase epsilon gene causes the cardiorenal pathology seems unlikely. Reversal of disease phenotype following manipulations by circadian principles would not be likely if it was a gene effect, nor would disease pathophysiology be confined to the heterozygote phenotype. The rationale is best illustrated both by the pathologic findings, and also the physiologic parameters represented in Fig. 4. These show that it is only the *tau*/+ animals, and only those aged in the desynchronous 24h environment, that develop cardiorenal disease. Additional support comes from when *tau*/+ hamsters are influenced by constant light; longevity is similar to wild type (7). Finally, we further show here that when the SCN is ablated in *tau*/+ heterozygotes, the influence of the

SCN is removed, and presumably the peripheral oscillators become free to operate at their intrinsic period defined by their molecular clock. Thus collectively the findings in this study show that in the absence of the SCN, the peripheral oscillators are free to operate as though they are in constant conditions. In the presence of disruptive signals from the SCN, this disturbs organ structure and function, and producing cardiorenal disease and leading to reduced longevity.

The downstream biochemical effects of clock disruption in heart and kidney are not defined. As yet we have only embryonic knowledge of the steps by which clock time is actually translated into the molecular events that control cell structure and function, and in particular, in the cardiorenal system. One possible candidate link is through perturbation of the glycogen synthase kinase -3-β (GSK3β) system; it plays an important regulatory role in cardiac hypertrophy through the stabilization or degradation of β-catenin via ubiquitination and the 26S proteasome(1, 8-10). We speculate on the GSK3β molecule as one potential avenue for future investigation as it has also most recently been reported to be involved in modulation of circadian molecular clock pathways; however, further investigation is beyond the scope of this study. Additional and possibly congruent pathways may involve the cardiomyocyte CLOCK and myocardial metabolism, as is being pursued by others(4). Finally, we recently report that circadian rhythm disruption exacerbates preexisting heart disease in a murine model of pressure overload hypertrophy(15), mediated in part by altered rhythmic gene expression. It is also likely that altered autonomic bias, and especially cardiac sympathetic tone, and cycling of neurohormones relevant to the cardiovascular system play a role; these clearly warrant future investigation. Further support of this notion of an autonomic bias or possibly even sympathetic neurotransmitters acting on cardiomyocytes has been suggested by studies using myocyte culture *in vitro*(3). Moreover, neuro/hormonal factors are also implicated as major contributors to the circadian timing of onset of adverse cardiovascular events such as myocardial infarction and sudden cardiac death. Thus taken together, our findings support the notion that not only is physiology rhythmic, but they furthermore illustrate that the processes that trigger compensatory changes in cardiovascular *disease* are rhythmic as well.

Circadian coordination of daily physiology is critical to the integrity of peripheral organs such as the heart and kidney. The results of these studies suggest that that the long term

disruption of circadian rhythms, for example in shiftworkers, transoceanic flight attendants or patients with sleep disturbances, can ultimately result in heart and kidney disease. These results have enormous implications for public health and the pathogenesis of cardiac and renal disease; they indicate that maintaining normal circadian rhythms may be an important long term lifestyle measure for the prevention of these diseases.

Perspectives and Significance

Circadian rhythmicity has been extensively characterized at the level of the SCN, followed by recent investigations that add focus to the peripheral system. It is widely suggested that circadian rhythms of behavior and physiology play a crucial role in integrative physiology, and concomitant organ health and integrity. The cardiovascular system is of particular interest as downstream target of circadian regulation, as has been indicated in numerous epidemiologic and clinical physiology reports. We now demonstrate experimentally that normal cardiac physiology, and conversely development of cardiac pathophysiology, may be explained by coincidence between internal and external circadian cues. This is shown in *tau*/+ hamsters, where there is desynchrony between the 22h internal endogenous clock system, and entrainment to the external 24h L:D environment. Furthermore these data support the very recent notion demonstrated using algae and plants(13, 17, 22), that circadian regulation is integral to the fitness and growth of an organism. Thus this study shows that circadian dysregulation – desynchrony between the internal circadian clock system and entrainment to normal L:D – can play an etiologic role in the development of cardiac disease.

FIGURE LEGENDS

Figure 1. Development of profound cardiac hypertrophy in *tau*/+ circadian mutant hamsters. **(a)** Representative genotype versus circadian phenotype shows wt, *tau*/+, and *tau/tau* hamsters analyzed for the mutation in the CK1e, on 1% EtBr agarose gel analysis. **(b)** Representative phenotype by activity analysis shows earlier onset and fractured activity pattern in *tau*/+ hamsters (left) entrained to LD 14:10, and reduced 22h circadian period in DD (<4 lux), as compared to wildtypes (24h, right). **(c)** Representative images of hearts from *tau*/+ show extensive pathology; widespread mocyte hypertrophy *(Ci,* Masson's trichrome) and myocardial fibrosis *(Cii,* Picrosirius red). **(d)** Representative images from wildtype hearts *(Di, Dii)* shown at the same magnification, which have no obvious signs of pathology. **(e)** Digital quantification demonstrates significant myocardial fibrosis (n=10, $P<0.01$) in *tau*/+ heart. **(f)** Increased myocyte cross sectional area (MCSA) (n=40, $P<0.05$) in *tau*/+ hearts. **(g)** Increased heart weight in *tau*/+ animals. **(h)** Heart:body weight ratio consistent with development of gross cardiac hypertrophy. Values are listed in Tables 1-3.

Figure 2. The *tau*/+ have severe heart disease and evidence of underlying kidney disease. Renal pathology in *tau*/+ (left) versus w (right), showing **(a)** tubular dilatation in *tau*/+ kidney (periodic acid stain), and **(b)** widespread fibrosis with collagen deposition in *tau*/+ kidney (Picrosirius red). **(c)** Electron microscopy shows glomerular ischemia, but no evidence of immune-type deposits in tau/+ kidney. This is consistent with development of primary renal disease, and helps exclude infection or autoimmune activity as cause.

Figure 3. Mass spectrometry proteomics and apoptosis in *tau*/+ kidneys. **(a)** Proteinuria in *tau*/+ urine by 17 months of age (white=4 months, black=17 months of age). **(b)** Representative urine samples analyzed by gel electrophoresis revealing the presence of both high and low molecular weight proteins in the *tau*/+ urine. First lane is marker, and subsequent lanes represent different animals. Two arrows denoted on the right side of the gels; top arrow is albumin, lower arrow points to an ~15kDa protein band appearing characteristically in urine of *tau*/+ animals. This band is excised, trypsin digested, and subject to mass spectrometry analyses. **(c)** Representative MS/MS spectrum for the 15kDa band, identified by mass spectrometry as *cytochrome c*, a marker of apoptosis. **(d)** TUNEL staining revealing apoptosis in *tau*/+ mutant kidney (n>3). Apoptosis was detected in kidney

sections taken from the aging tau heterozygote hamsters. Apoptosis was not detected in age-matched wild-type kidney sections. The inset is a positive control using murine thymus.

Figure 4. Rescue of circadian disturbance protects against the cardiac disease phenotype. **(a)** Representative locomotor activity showing a tau of 22h for *tau*/+ in LD 12:10. **(b)** Normal cardiac histologic sections from aged *tau*/+ maintained on a phenotype-appropriate 22h LD; these animals exhibit healthy myocardium (Masson's trichrome). **(c)** Renal pathology is also normal, as shown here from aged *tau*/+ maintained on a phenotype-appropriate 22h LD cycle (periodic acid stain). **(d)** Renal histologic sections from aged tau/+ on 22h LD further revealing no evidence of fibrosis or collagen deposition; the kidneys appear normal (Picrosirius red). **(e-h)** Cardiac indices in aged *tau*/+ maintained in 22h LD. **(e)** Normal left ventricular end diastolic dimensions (LVEDD, mm) in 22h *tau*/+ at 17 months of age. **(f)** Normal left ventricular end systolic dimensions (LVESD, mm) in 22h tau/+ at 17 months of age. **(g)** Normal mean arterial blood pressure (MABP, mmHg) with no evidence of hypotension in 22h *tau*/+ at 17 months of age. **(h)** The % fractional shortening (%FS) in 22h *tau*/+ revealing normal contractility and consistent with hemodynamic and morphometric parameters. All phenotypes tested are shown, with black lines=22h *tau*/+, red=24h *tau*/+, blue= *tau/tau*, green=wt. Results plotted as mean±SEM at 4 and 17 months of age (see Tables for data). Plasma and/or urinary biochemistry levels remain normal in *tau*/+ maintained on the 22h L:D cycle, as compared to the abnormal levels for *tau*/+ on 24h L:D (as in Figure 3A, Table 3). Statistical significance *=P<0.01 evaluated by ANOVA.

Figure 5. SCN lesions prevent or reverse circadian rhythm related cardiac hypertrophy. The SCN in young adult hamsters (6 months of age) carrying the *tau* mutation (+*/tau)* are electrically ablated, and then animals are maintained in an LD14:10 light cycle thereafter. When animals are close to death as determined by animal care staff, they are removed, euthanized, and the heart weight to body weight ratio is determined. Control animals are wild type and intact *tau*/+ housed side by side in the same lighting conditions. N=6 per group. **(a)** HW/BW ratios for WT, +/*tau* (intact), and +/*tau* (SCNX). The effectiveness of SCN lesions are verified by the lack of rhythmic wheel running behavior. **(b)** Actogram shows the immediate (4 month) and long term (16 month) result of the lesion. Animals are housed in LD14:10 following surgery.

REFERENCES

1. **Antos CL, McKinsey TA, Frey N, Kutschke W, McAnally J, Shelton JM, Richardson JA, Hill JA, and Olson EN.** Activated glycogen synthase-3 beta suppresses cardiac hypertrophy in vivo. *Proc Natl Acad Sci U S A* 99: 907-912, 2002.
2. **Bradley TD and Floras JS.** Sleep apnea and heart failure: Part II: central sleep apnea. *Circulation* 107: 1822-1826, 2003.
3. **Durgan DJ, Hotze MA, Tomlin TM, Egbejimi O, Graveleau C, Abel ED, Shaw CA, Bray MS, Hardin PE, and Young ME.** The intrinsic circadian clock within the cardiomyocyte. *Am J Physiol Heart Circ Physiol* 289: H1530-1541, 2005.
4. **Durgan DJ, Trexler NA, Egbejimi O, McElfresh TA, Suk HY, Petterson LE, Shaw CA, Hardin PE, Bray MS, Chandler MP, Chow CW, and Young ME.** The circadian clock within the cardiomyocyte is essential for responsiveness of the heart to fatty acids. *J Biol Chem*, 2006.
5. **Fukuhara C and Tosini G.** Peripheral circadian oscillators and their rhythmic regulation. *Front Biosci* 8: d642-651, 2003.
6. **Furlan R, Barbic F, Piazza S, Tinelli M, Seghizzi P, and Malliani A.** Modifications of cardiac autonomic profile associated with a shift schedule of work. *Circulation* 102: 1912-1916, 2000.
7. **Guo YF and Stein PK.** Circadian rhythm in the cardiovascular system: chronocardiology. *Am Heart J* 145: 779-786, 2003.
8. **Haq S, Michael A, Andreucci M, Bhattacharya K, Dotto P, Walters B, Woodgett J, Kilter H, and Force T.** Stabilization of beta-catenin by a Wnt-independent mechanism regulates cardiomyocyte growth. *Proc Natl Acad Sci U S A* 100: 4610-4615, 2003.
9. **Hardt SE and Sadoshima J.** Glycogen synthase kinase-3beta: a novel regulator of cardiac hypertrophy and development. *Circ Res* 90: 1055-1063, 2002.
10. **Hino S, Michiue T, Asashima M, and Kikuchi A.** Casein kinase I epsilon enhances the binding of Dvl-1 to Frat-1 and is essential for Wnt-3a-induced accumulation of beta-catenin. *J Biol Chem* 278: 14066-14073, 2003.
11. **Hurd MW and Ralph MR.** The significance of circadian organization for longevity in the golden hamster. *J Biol Rhythms* 13: 430-436, 1998.
12. **Ito T, Ishida N.** Circadian rhythm orchestrates the cell cycle of rat renal epithelial cells: A novel mechanism to regulate the cell cycle. *Kidney International* 68: 1965, 2005.
13. **Johnson CH.** Endogenous timekeepers in photosynthetic organisms. *Annu Rev Physiol* 63: 695-728, 2001.
14. **Martino T, Arab S, Straume M, Belsham DD, Tata N, Cai F, Liu P, Trivieri M, Ralph M, and Sole MJ.** Day/night rhythms in gene expression of the normal murine heart. *J Mol Med* 82: 256-264, 2004.
15. **Martino T, Tata N, Belsham, DD., Chalmers, J., Straume, M., Lee, P., Pribiag, H., Khaper, N., Liu, PP., Dawood, F., Backx, PH., Ralph, MR., Sole, MJ.** Disturbed Diurnal Rhythm Alters Gene Expression and Exacerbates Cardiovascular Disease with Rescue by Resynchronization. *Hypertension* 49: 1-10, 2007.
16. **Muller JE, Tofler GH, and Stone PH.** Circadian variation and triggers of onset of acute cardiovascular disease. *Circulation* 79: 733-743, 1989.

17. **Nozue K, Covington MF, Duek PD, Lorrain S, Fankhauser C, Harmer SL, and Maloof JN.** Rhythmic growth explained by coincidence between internal and external cues. *Nature*, 2007.
18. **Osiel S, Golombek DA, and Ralph MR.** Conservation of locomotor behavior in the golden hamster: effects of light cycle and a circadian period mutation. *Physiol Behav* 65: 123-131, 1998.
19. **Penev PD, Kolker DE, Zee PC, and Turek FW.** Chronic circadian desynchronization decreases the survival of animals with cardiomyopathic heart disease. *Am J Physiol* 275: H2334-2337, 1998.
20. **Ralph MR and Menaker M.** A mutation of the circadian system in golden hamsters. *Science* 241: 1225-1227, 1988.
21. **Storch KF, Lipan O, Leykin I, Viswanathan N, Davis FC, Wong WH, and Weitz CJ.** Extensive and divergent circadian gene expression in liver and heart. *Nature* 417: 78-83, 2002.
22. **Woelfle MA, Ouyang Y, Phanvijhitsiri K, and Johnson CH.** The adaptive value of circadian clocks: an experimental assessment in cyanobacteria. *Curr Biol* 14: 1481-1486, 2004.
23. **Young ME, Razeghi P, Cedars AM, Guthrie PH, and Taegtmeyer H.** Intrinsic diurnal variations in cardiac metabolism and contractile function. *Circ Res* 89: 1199-1208, 2001.
24. **Young ME, Razeghi P, and Taegtmeyer H.** Clock genes in the heart: characterization and attenuation with hypertrophy. *Circ Res* 88: 1142-1150, 2001.

Table 1. Echocardiographic, hemodynamic and morphometric parameters in +/tau mutant hamsters (17 months of age)

	+/+	+/*tau* (14:10)	+/*tau* (12:10)
N	8	8	8
HR (bpm)	413±8	422±11	404±13
AW (mm)	1.18±0.02	1.15±0.03	1.16±0.04
LVEDD (mm)	5.82±0.06	6.36±0.11*	5.48±0.12¶
LVESD (mm)	3.13±0.09	4.47±0.05*	3.07±0.08¶
FS (%)	46.3±1.3	29.7±2.4*	43.9±2.4¶
VCFc (circ/s)	8.36±0.26	4.95±0.54*	8.05±0.31¶
PAV (cm/s)	89±2	73.9±1.8*	88±3.1¶
SBP (mmHg)	146±3	117±5*	150±3¶
DBP (mmHg)	94±3	68±4*	93±1¶
MABP (mmHg)	111±3	84±4*	112±2¶
$+dP/dt_{max}$ (mmHg/sec)	9987±441	6118±373*	9182±331¶
$-dP/dt_{max}$ (mmHg/sec)	9929±396	6003±271*	9226±946¶
LVEDP (mmHg)	3.8±0.8	10.4±1.5*	-5.2±0.7¶
BW (g)	138±2.4	124±7.6	131±1.7
HW/BW (mg/g)	4.37±0.09	6.58±0.52*	5.15±0.16¶
HW/TL (mg/mm)	26.4±1.1	35.7±1.5*	32.2±0.6¶
KW/BW (mg/g)	5.02±0.21	5.81±0.41	5.06±0.13
KW/TL (mg/mm)	29.2±1.8	31.2±1.6	31.7±0.4
Fibrosis (pixels)	28783±9614	58132±7928#	36879±3740¶
MCSA (μm^2) (n=40)	271±6.2	366±9.6*	310±8.7¶

*=p<0.01 and #=p<0.05 compared with all other groups (wt, +/*tau, tau/tau*); ¶=p<0.05 17 month +/tau (12:10) compared with 17mo +/tau (14:10); values are mean±SEM; values for *tau/tau* are in Supplementary Table 1; LVEDD=left-ventricular end diastolic dimension; LVESD=left-ventricular end systolic dimension; FS=fractional shortening (LVEDD-LVESD)/LVEDDx100); VCFc=velocity of circumferential shortening (FS/ET); HWBW, KWBW=heart weight/body weight, kidney weight/body weight; HWTL, KWTL=heart weight/tibial length, kidney weight/tibial length; Fibrosis (cardiac); MCSA=myocyte cross sectional area.

Table 2. Echocardiographic, hemodynamic and morphometric parameters in young *tau* hamsters

	+/+ (4mo)	+/*tau* (4mo)
	6	6
HR (bpm)	404±6	411±5
AW (mm)	0.98±0.05	1.03±0.06
LVEDD (mm)	5.19±0.1	5.41±0.11
LVESD (mm)	2.84±0.11	3.08±0.09
FS (%)	45.8±1.8	43.1±3.1
VCFc (circ/s)	8.52±0.36	8.22±0.63
PAV (cm/s)	85±3.5	82±2.8
SBP (mmHg)	135±5	147±3
DBP (mmHg)	87±4	97±2
MABP (mmHg)	103±4	114±2
$+dP/dt_{max}$ (mmHg/sec)	10942±591	8595±636
$-dP/dt_{max}$ (mmHg/sec)	10920±400	7425±1807
LVEDP (mmHg)	-1.3±0.9	0.5±1.7
BW (g)	113±5.2	113±3.7
HW/BW (mg/g)	4.91±0.13	4.72±0.2
HW/TL (mg/mm)	24.33±1.9	23.25±1.1
KW/BW (mg/g)	5.3±0.28	5.38±0.25
KW/TL (mg/mm)	26.1±2.1	26.78±1.9
Fibrosis (pixels)	8698±435	9013±481
MCSA (μm^2) (n=40)	239±10.3	256±8.5

#=p<0.05 compared with 17mo wildtype group; values are mean±SEM; LVEDD=left-ventricular end diastolic dimension; LVESD=left-ventricular end systolic dimension; FS=fractional shortening (LVEDD-LVESD)/LVEDDx100); VCFc=velocity of circumferential shortening (FS/ET); HWBW, KWBW=heart weight/body weight, kidney weight/body weight; HWTL, KWTL=heart weight/tibial length, kidney weight/tibial length; cardiac fibrosis; MCSA=myocyte cross sectional area.

Table 3. Plasma biochemistry in *tau* hamsters

	Na^+ (mM)	K^+ (mM)	Cl^- (mM)	Ca^{2+} (mM)	Lactate (mM)	RBG (mM)	Urea (mM)	Cr (mM)
+/tau (17mo)	140.5±1.4	6.12±0.38*	102.5±0.8	1.22±0.04	5.21±0.47	9.45±0.9	6.8±0.56	112.4±8.1*
+/+ (17mo)	138.8±0.7	5.06±0.11	101.2±0.5	1.21±0.02	6.06±0.41	9.23±0.89	6.36±0.67	72.5±2.7
+/tau (4 mo)	139.3±0.5	5.0±0.2	104.0±0.49	0.77±0.04	9.8±0.32	13.71±1.1	7.6±0.29	69.6±4.68
+/+ (4 mo)	137.3±1.1	4.8±0.2	105.3±1.6	0.87±0.05	8.7±0.72	10.21±1.06	7.2±0.35	78.9±6.67

Blood samples were collected from anesthesized hamsters at ZT12-16 and 200 µl of plasma was used for measurement of plasma Na^+, K^+, Cl^-, ionized Ca (Ca^{2+}), lactate, glucose, urea and creatinine using a Stat Profile M7 Analyzer (Nova Biomedical Corp., Waltham, Massachusetts, USA). n≥7 per timepoint; RBG=random blood glucose; values are mean±SEM; *p<0.01 compared to all other groups.

Figure 1

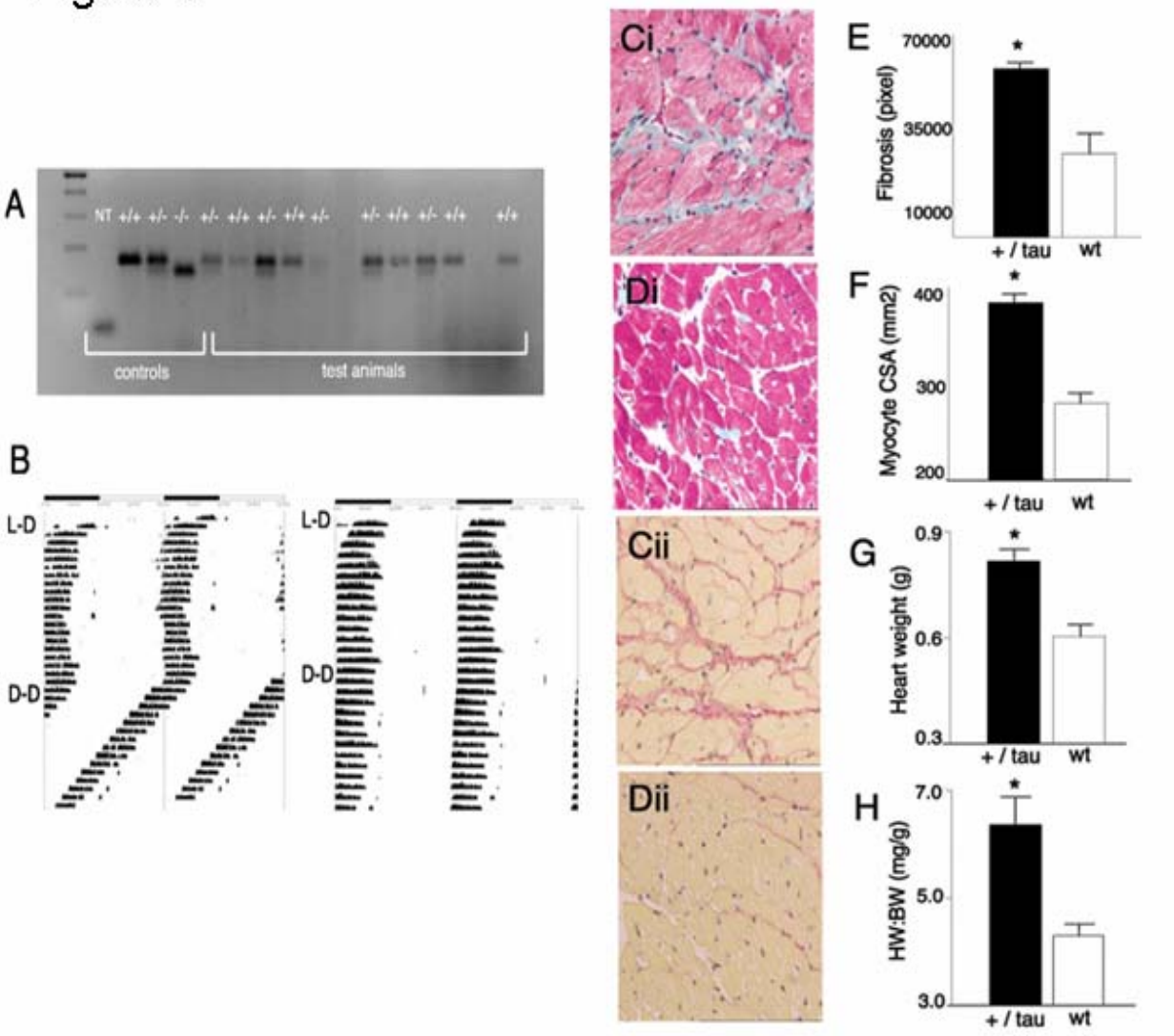
A
NT +/+ +/- -/- +/- +/+ +/- +/+ +/- +/- +/+ +/- +/+ +/+
controls
test animals
B
L-D
D-D
L-D
D-D
Ci
Di
Cii
Dii
E
Fibrosis (pixel)
70000
35000
10000
+ / tau
wt
F
Myocyte CSA (mm2)
400
300
200
+ / tau
wt
G
Heart weight (g)
0.9
0.6
0.3
+ / tau
wt
H
HW:BW (mg/g)
7.0
5.0
3.0
+ / tau
wt

Figure 2

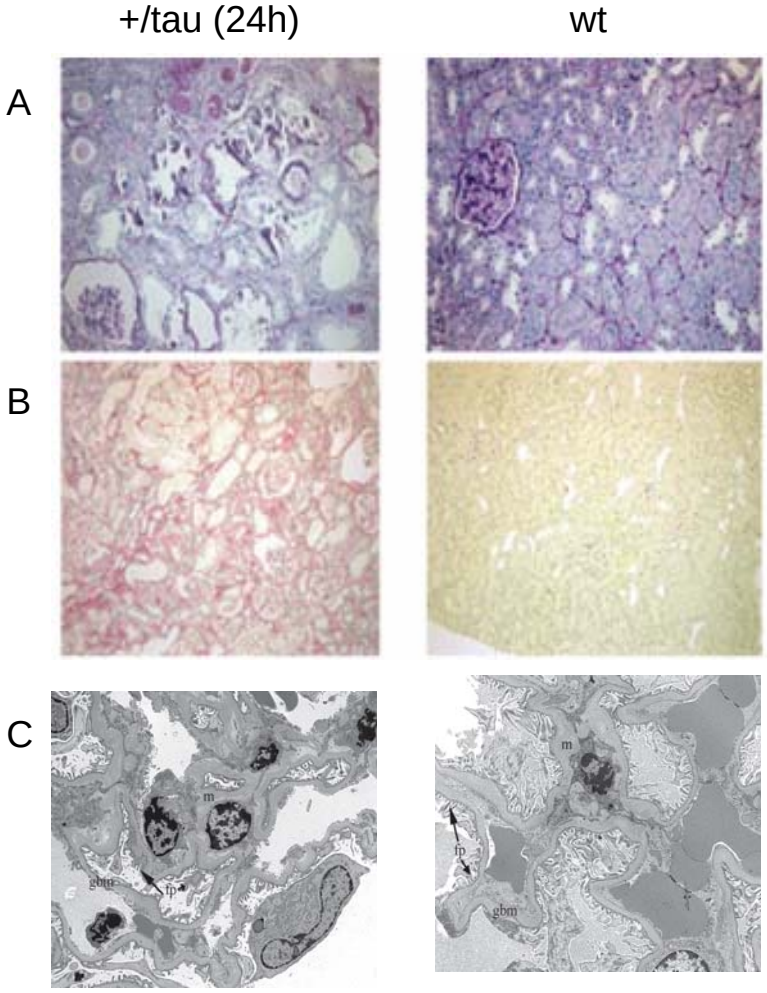

Figure 3

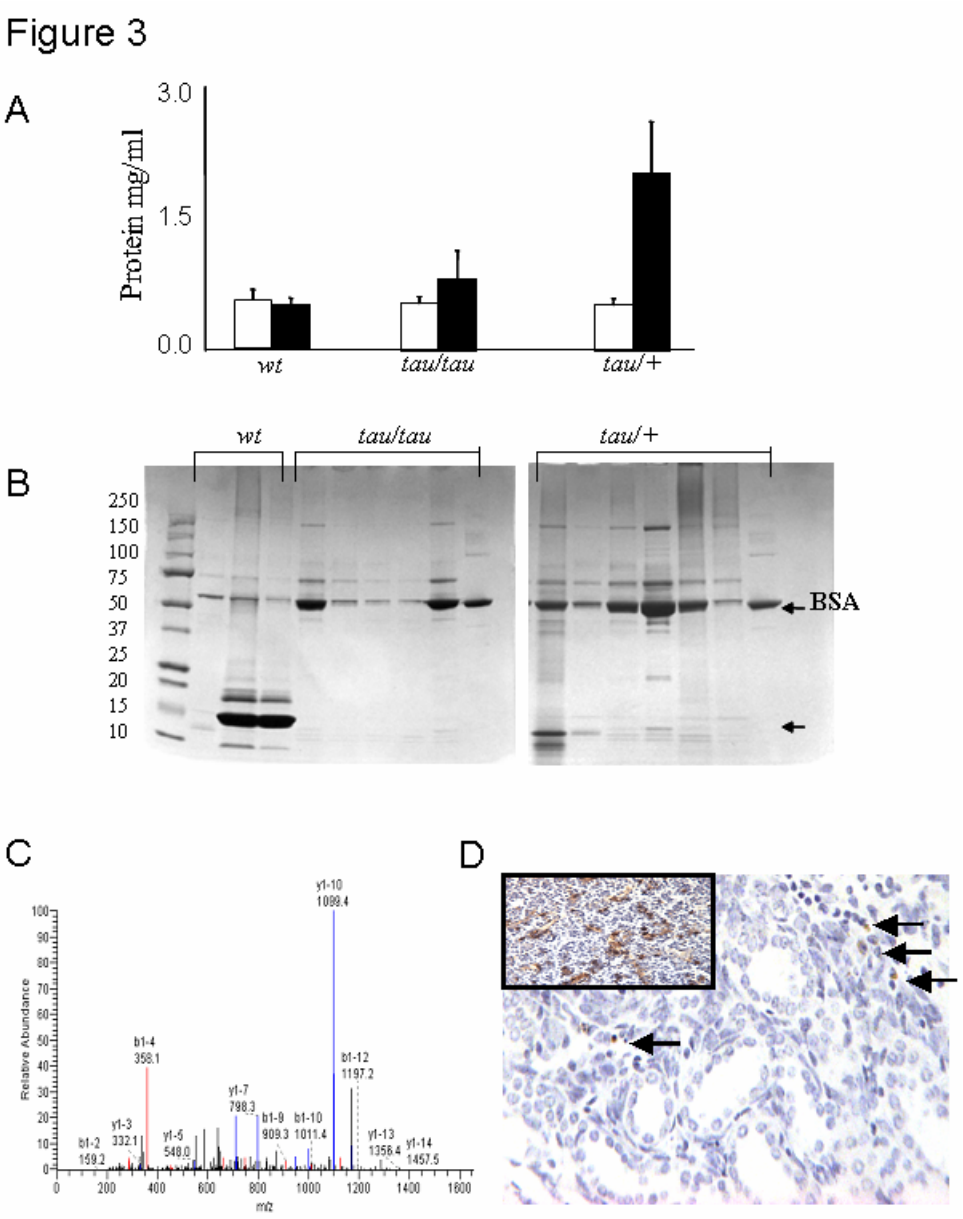
A
3.0
1.5
0.0
Protein mg/ml
wt
tau/tau
tau/+
B
wt
tau/tau
tau/+
250
150
100
75
50
37
25
20
15
10
BSA
C
Relative Abundance
m/z
y1-10
1099.4
b1-4
358.1
b1-12
1197.2
y1-7
798.3
b1-9
909.3
b1-10
1011.4
y1-3
332.1
y1-5
548.0
y1-13
1358.4
y1-14
1457.5
b1-2
159.2
D

Figure 4

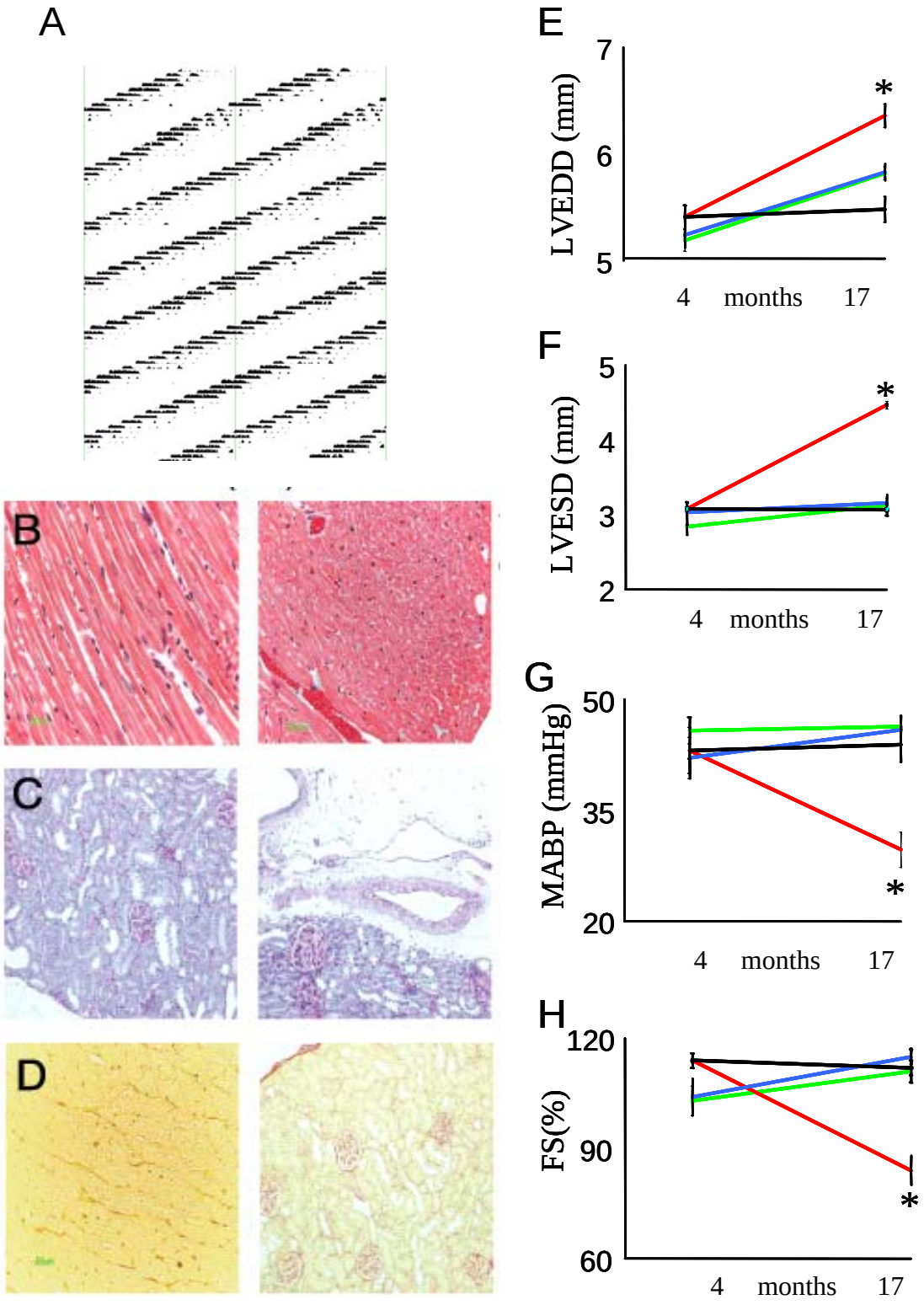
A
B
C
D
E
LVEDD (mm)
7
6
5
4
months
17
F
LVESD (mm)
5
4
3
2
4
months
17
G
MABP (mmHg)
50
35
20
4
months
17
H
FS(%)
120
90
60
4
months
17

Figure 5